The solar seeing monitor MISOLFA: presentation and first results

Irbah A. [a] Corbard T. [b] Assus P. [b] Borgnino J. [c] Dufour C. [a] Ikhlef R. [d] Martin F. [b] Meftah M. [a] Morand F. [b] Renaud C. [b] and Simon E. [b]

[a] Université Versailles St-Quentin; CNRS/INSU, LATMOS-IPSL, Guyancourt, France

[b] Université de Nice Sophia Antipolis, CNRS, Observatoire de la Côte d'Azur, BP 4229 06304 Nice Cedex 4, France

[c] Université de Nice-Sophia Antipolis, UMR 6525 Astrophysique, Parc Valrose F-06108 Nice Cedex 2, France

[d] CRAAG - Observatoire d'Alger BP 63 Bouzaréah Alger, Algérie

ABSTRACT

PICARD is a space mission developed to observe the Sun at high angular resolution. One of the main space objectives of PICARD is to measure the solar diameter with few milli arc-seconds accuracy. A replica of the space instrument will be installed at Calern Observatory in order to test our ability to make such measurement from ground with enough accuracy. High angular resolution observations with ground-based instrument are however limited by atmospheric turbulence. The seeing monitor MISOLFA is developed to give all observation conditions at the same moments when solar images will be recorded with the twin PICARD instruments. They will be used to link ground and space measurements. An overview of the PICARD mission and the solar ground-based experiments will be first given. Optical properties of MISOLFA will be after presented. The basic principles to measure atmospheric parameters and the methods used to obtain them from solar images will be given. Finally, some recent results obtained at Calern Observatory will be presented and discussed.

Keywords: Atmospheric turbulence, seeing monitor, Sun

1. INTRODUCTION

Observations of the Sun at High Angular Resolution using ground-based telescopes need an accurate modelling of the optical effects induced by atmospheric turbulence. In fact, a diameter measurement analysis revealed a dependence with the seeing condition as represented by Fried's parameter r_0.[1] Numerical simulations were developed in order to better understand atmospheric effects on diameter measurements. The error decreases with the seeing but it is also strongly conditioned by the turbulence coherence times.[2] The error shows also a weak dependence with the outer scale $\mathcal{L}_0$ for a small aperture telescope. A seeing monitor is then useful and MISOLFA is built for this goal. MISOLFA is a generalized daytime seeing monitor that will observe together with SODISM II, replica of the PICARD space instrument, which will be operational in space in 2010. The main objectives are the comparison of the results deduced from spatial and ground data as well as the evaluation of the atmospheric turbulence optical effects on the measurements performed from the ground. This instrument is developed for solar diameter measurements and will be based at Calern Observatory (Observatoire de la Côte dAzur). MISOLFA will give in real time estimations of the coherence parameters characterizing wave-fronts degraded by atmospheric turbulence (Fried's parameter r_0, size of the isoplanatic patch θ_0, spatial coherence outer scale $\mathcal{L}_0$ and atmospheric correlation times). The monitor will also estimate optical turbulence profiles. The monitor proposed here is founded on the observation of Angle-of-Arrival (AA) fluctuations (solar limb image motion) and their statistical analysis.

2. THE SODISM INSTRUMENT OF THE PICARD MISSION

The PICARD payload consists in absolute radiometers and photometers measuring the total solar irradiance and SODISM which is an imaging telescope developed to determine the diameter, the limb shape and the asphericity of the Sun.[3] SODISM (Solar Diameter Imager and Surface Mapper) makes an image of the Sun on a CCD detector. Wavelengths are selected by interference filters placed on 2 wheels. Wavelength domains are chosen free of Fraunhofer lines (535.7, 607.1 and 782.2 nm). Active regions are detected in the 215 nm domain and the CaII (393.37 nm) line. Helioseismologic observations are performed at 535.7 nm.[4] The satellite platform is stabilized at 36 arc-seconds. The telescope primary mirror stabilizes then the Sun image within 0.2 arcsecond using piezo electric actuators. An internal calibration system composed with 4 prisms, allows to follow scale factor variations induced by instrument deformations resulting from temperature fluctuations in orbit or others causes.[5] The diameter measurements are referred to star angular distances by rotating the spacecraft towards some doublet stars several times per year. The instrument stability is assured by use of stable materials (Zerodur for mirrors, Carbon-Carbon and Invar for structure). The whole instrument is temperature stabilized within 1^oC. The CCD is also temperature stabilized around -13^oC within 0.2^oC. In order to limit the solar energy, a window is set at the telescope entrance limiting the input to 5% of the total solar irradiance. No significant ageing has been measured in laboratory for the duration of the mission. The optical scheme of SODISM is shown in Fig. 1. It is a similar instrument as SODISM, that will be installed at Calern Observatory (Observatoire de la Côte dAzur).
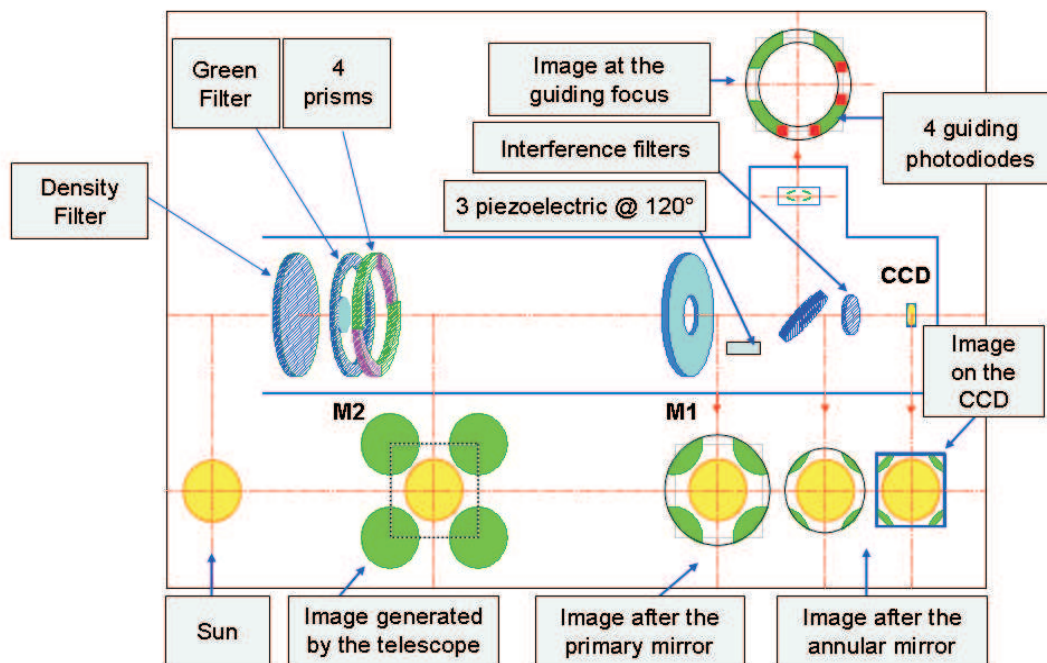

Figure 1. SODISM optical scheme.

3. EXPERIMENTAL CONCEPT - OBSERVATION OF THE AA-FLUCTUATIONS

The Angle-of-Arrival fluctuations, which are fluctuations of the normal to the perturbed wavefronts, can directly be observed in the image plane (this is the case of Shack-Hartmann's sensors currently used in the adaptive optics systems). But, they can also be shown in the pupil plane, for example, when the astronomical sources observed (Sun or Moon) present an intensity distribution with a strong discontinuity.[6] In this case, an analysis of the perturbed wavefronts analog to a Foucault test can be performed. Figure 2 shows the principle of the monitor experimental device. It consists in 2 ways. The first one named in the following *image plane observation way*, allows recording directly the AA-fluctuations using a CCD camera placed on the solar limb image (N^o1).
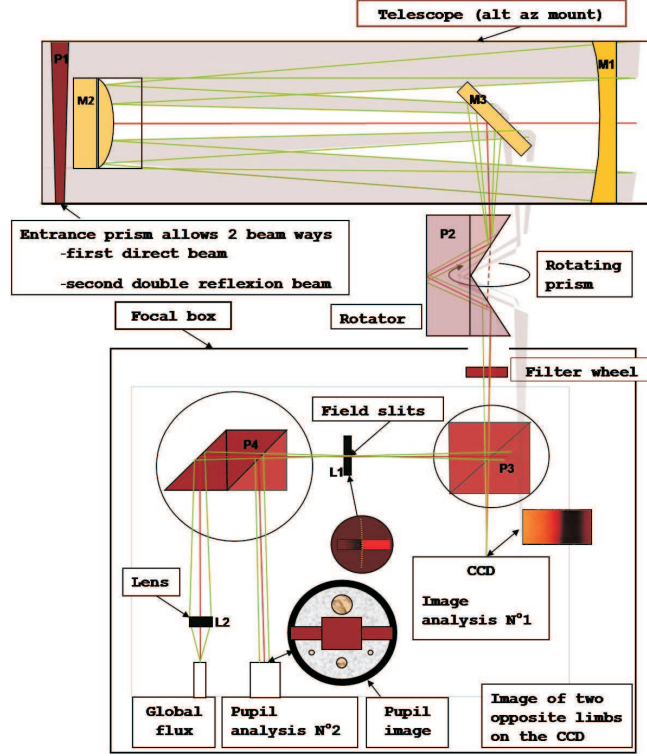
Figure 2. MISOLFA : experimental device.

A beam splitter allows to create a second way named in the following *pupil plane observation way* in which the telescope pupil (P1) is observed by means of a lens through a narrow slit placed on the solar limb image (N°2). The diaphragm size is some arc-seconds wide and about fifty arcseconds length. The pupil image intensity present fluctuations which are proportional to the AA-fluctuations (see section 4). Several photodiodes allow recording the intensity fluctuations with optical fibers positioned on the image behind diaphragms of different sizes. The signals given by the different photodiodes will be simultaneously recorded and a spatiotemporal analysis performed.

4. THEORETICAL MODELS AND TURBULENCE PARAMETER ESTIMATION

4.1 The image plane observation way

The theoretical results presented in this section have been obtained in the same way than those used to interpret the nighttime observation data given by the Generalized Seeing Monitor.[7,8] The transverse spatial covariance of the AA-fluctuations observed at a distance B with 2 telescopes of diameter D may is expressed in the case where the atmospheric turbulence is described by the Von Kàrmàn model as:[9]

$$C_\alpha(\overrightarrow{B}) = 0.0716\lambda^2 r_0^{-\frac{5}{3}} \int_0^{+\infty} df f^3 (f^2 + \frac{1}{\mathcal{L}_0{}^2})^{-\frac{11}{6}} [J_0(2\pi f(B)) + J_2(2\pi f(B))][\frac{2J_1(\pi Df)}{\pi Df}]^2 \qquad (1)$$

where f is an angular frequency, λ the wavelength and J_0, J_1, J_2 are Bessel functions of the first kind. The spatial coherence inner scale is taken equal to 0 in the Von Kàrmàn model.

It is easy to deduce the transverse angular covariance replacing B by θh in Equation (1).[10,11] This means that observations are performed with a single telescope (pupil of diameter D) in 2 directions in the sky separated by θ. h is the altitude of an equivalent impulse layer giving same optical effects at ground level than the whole turbulent terrestrial atmosphere. This leads to :

$$\mathcal{C}_\alpha(\theta) = 0.0716\lambda^2 r_0^{-\frac{5}{3}} \int_0^{+\infty} df f^3 (f^2 + \frac{1}{\mathcal{L}_0{}^2})^{-\frac{11}{6}} [J_0(2\pi f\theta h) + J_2(2\pi f\theta h)][\frac{2J_1(\pi Df)}{\pi Df}]^2 \qquad (2)$$

Equation 2 allows to estimate by the inversion technique presented in Seghouani *et al.*,[10] the Fried parameter r_0, the spatial coherence outer scale $\mathcal{L}_0$ and the isoplanatic angle θ_0 deduced from the ratio r_0/h. In the case of a multilayer turbulent atmosphere, we uses the expression of the transverse angular structure function, with the assumptions already given. It may be written as :

$$\mathcal{C}_\alpha(\theta) = 1.19 \int_0^{+\infty} dh C_n^2(h) \int_0^{+\infty} df f^3 (f^2 + \frac{1}{L_0(h)^2})^{-\frac{11}{6}} [J_0(2\pi f\theta h) + J_2(2\pi f\theta h)][\frac{2J_1(\pi Df)}{\pi Df}]^2 \tag{3}$$

where $C_n^2(h)$ is the energy vertical profile of the " optical " turbulence given by the structure constant for the air refractive index fluctuations and $L_0(h)$ is the turbulent outer scale vertical profile.
The transverse angular structure function is given by :

$$d_\alpha(\theta) = 2[\sigma_\alpha^2 - \mathcal{C}_\alpha(\theta)] \tag{4}$$

where $\sigma_\alpha^2 = C_\alpha(0)$. Introducing (3) in Equation (4) leads to :

$$d_\alpha(\theta) = 2.4 \int_0^{+\infty} dh C_n^2(h) \int_0^{+\infty} df f^3 (f^2 + \frac{1}{L_0(h)^2})^{-\frac{11}{6}} [1 - J_0(2\pi f\theta h) - J_2(2\pi f\theta h)][\frac{2J_1(\pi Df)}{\pi Df}]^2 \tag{5}$$

As a first approach we can consider the case in which $L_0(h) = \infty$ for which the optical turbulence profile $C_n^2(h)$ can be estimated by application of the inversion technique described in Bouzid *et al.*[11]

4.2 The pupil-plane observation way

The evolution characteristic times of the AA-fluctuations will be estimated using the pupil-plane observation way thanks to its high acquisition rate. Geometrical optics is helpful to understand how AA-fluctuations are put in evidence in the pupil plane. Light rays of the atmospheric perturbed wavefront undergo random angles and pass or no through the diaphragm. The pupil illumination observed through the diaphragm will then be related to the local slopes of the wave-front. Intensity variations in the pupil-plane image are therefore directly related to AA-fluctuations at the telescope entrance pupil when an extended source is observed. Previous works have shown the goodness of the linear relationship between intensity and AA-fluctuations.[12, 13] We recall hereafter the formalism explaining this proportional relationship.[14]
We consider first a monochromatic wave incoming from a given point-source situated in the $\overrightarrow{\alpha_0}$ angular direction. The complex amplitude of such a wave may be expressed at the ground level as $\sqrt{I_0(\overrightarrow{\alpha_0})}\psi_{\overrightarrow{\alpha_0}}(\overrightarrow{r})\exp(\frac{2\pi i}{\lambda}\overrightarrow{\alpha_0}\overrightarrow{r})$ where $\overrightarrow{r}$ is a space vector in the pupil-plane with coordinates (x, y), λ the monochromatic wave wavelength, $I_0(\overrightarrow{\alpha_0})$ an angular distribution of the incident light intensity and $\psi_{\overrightarrow{\alpha_0}}(\overrightarrow{r})$ is the normalized turbulence-disturbed complex amplitude of the light wave. The propagation trough the telescope of the wave-front limited to its entrance pupil forms a Fraunhoffer diffraction pattern in the instrument focal plane. The angular distribution $K_{\overrightarrow{\alpha_0}}(\overrightarrow{\alpha})$ is then expressed by :

$$K_{\overrightarrow{\alpha_0}}(\overrightarrow{\alpha}) \propto \int d\overrightarrow{r} P(\overrightarrow{r})\sqrt{I_0(\overrightarrow{\alpha_0})}\psi_{\overrightarrow{\alpha_0}}(\overrightarrow{r})\exp(\frac{2\pi i}{\lambda}\overrightarrow{\alpha_0}\overrightarrow{r})\exp(\frac{-2\pi i}{\lambda}\overrightarrow{\alpha}\overrightarrow{r}) \tag{6}$$

where $\overrightarrow{\alpha}$ is a two-dimensional angle and $P(\overrightarrow{r})$ the pupil function equal to one inside the pupil area and to zero outside. Equation 6 may be rewritten as :

$$K_{\overrightarrow{\alpha_0}}(\overrightarrow{\alpha}) \propto FT[P(\overrightarrow{r})\sqrt{I_0(\overrightarrow{\alpha_0})}\psi_{\overrightarrow{\alpha_0}}(\overrightarrow{r})\exp(\frac{2\pi i}{\lambda}\overrightarrow{\alpha_0}\overrightarrow{r})] \tag{7}$$

where FT denotes the Fourier Transform evaluated for the reduced space frequencies $\overrightarrow{r}/\lambda$: $TF[f(\overrightarrow{r})] = \int d\overrightarrow{r} f(\overrightarrow{r})\exp(\frac{-2\pi i}{\lambda}\overrightarrow{\alpha}\overrightarrow{r})$.

$K_{\overrightarrow{\alpha_0}}(\overrightarrow{\alpha})$ is a speckled angular distribution of complex amplitude centered in the $\overrightarrow{\alpha_0}$ direction. It is then more or less masked according to its position relatively to the diaphragm borders placed in the telescope focal plane.

The pupil-plane image is obtained operating an inverse Fourier Transform of the complex amplitude $K_{\overrightarrow{\alpha_0}}(\overrightarrow{\alpha})$ over the diaphragm. The complex amplitude $K'_{\overrightarrow{\alpha_0}}(\overrightarrow{r})$ in the pupil-plane image is then given by :

$$K'_{\overrightarrow{\alpha_0}}(\overrightarrow{r}) \propto FT^{-1}[G_s(\overrightarrow{\alpha})K_{\overrightarrow{\alpha_0}}(\overrightarrow{\alpha})] \tag{8}$$

where $G_s(\overrightarrow{\alpha})$ the diaphragm angular transmission. FT^{-1} denotes the inverse Fourier Transform: $FT^{-1}(F(\overrightarrow{\alpha})) = \int d\overrightarrow{\alpha} F(\overrightarrow{\alpha}) \exp(\frac{2\pi i}{\lambda}\overrightarrow{\alpha}\,\overrightarrow{r})$.

The partial masking of $K_{\overrightarrow{\alpha_0}}(\overrightarrow{\alpha})$ with the diaphragm $G_s(\overrightarrow{\alpha})$ will be more or less important depending directly of $\overrightarrow{r}$. Intensity fluctuations $I_{\overrightarrow{\alpha_0}}(\overrightarrow{r}) = |K'_{\overrightarrow{\alpha_0}}(\overrightarrow{r})|^2$ will be then observed in the pupil-plane image. They are what we call the *Flying Shadows* obtained for the incidence angle $\overrightarrow{\alpha_0}$.

The resulting intensity fluctuations in the pupil-plane image for an incoherent extended source is the summation of all point source intensity contributions over the angular field-of-view allowed by the optical system i.e. the diaphragm angular size:

$$I(\overrightarrow{r}) = \int d\overrightarrow{\alpha_0} I_{\overrightarrow{\alpha_0}}(\overrightarrow{r}) \propto \int d\overrightarrow{\alpha_0} G_s(\overrightarrow{\alpha_0})|FT^{-1}[G_s(\overrightarrow{\alpha})FT[P(\overrightarrow{r})\sqrt{I_0(\overrightarrow{\alpha_0})}\psi_{\overrightarrow{\alpha_0}}(\overrightarrow{r})\exp(\frac{2\pi i}{\lambda}\overrightarrow{\alpha_0}\overrightarrow{r})]]|^2 \tag{9}$$

Equation 9 is the basic mathematical model giving the intensity fluctuations in the pupil-image of an incoherent extended object. If the considered object is the solar limb assuming by the way that its intensity has a linear relationship with $|\overrightarrow{\alpha}|$ along the diaphragm length positioned following the x-direction in instrument focal plane, Equation 9 leads to:[15]

$$I(\overrightarrow{r}) \propto P(\overrightarrow{r})\frac{\partial\varphi(\overrightarrow{r}(x,y))}{\partial y} \tag{10}$$

where $\propto$ denotes the proportionality operator and $\varphi(\overrightarrow{r})$ is the perturbed wave-front phase at the telescope entrance pupil. The phase derivative fluctuations at each wave-front point correspond to AA-fluctuations. The pupil-image observation way introduce a spatial filtering in the image due to the diaphragm leading to measure AA-fluctuations in the y-direction (Figure 3). Berdja *et al.*[14] have shown the good linear relationship between AA-fluctuations and intensity fluctuations as modeled with Equation 10 when the solar limb is observed.
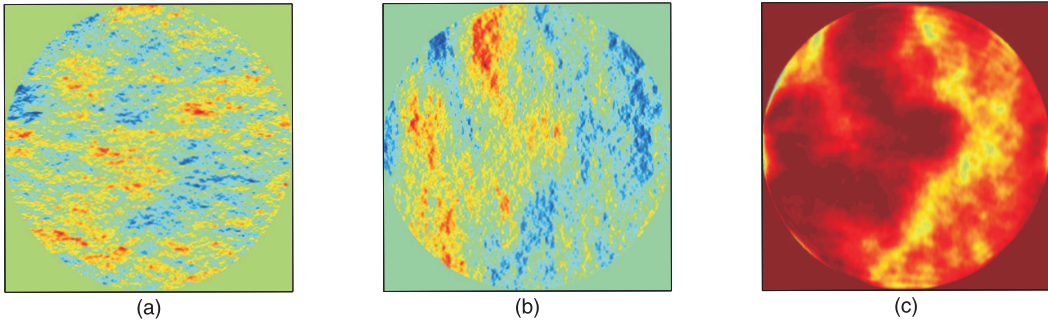

Figure 3. Simulated AA-fluctuations computed directly from the perturbed wave-front phase and observed as intensity fluctuations in pupil-plane image. (a) and (b) are respectively x and y AA components at the entrance pupil while (c) is the y component observed in the pupil-plane image as intensity fluctuations. The perturbed wave-front was simulated in the near-field approximation case considering $r_0 = 4cm$, $\mathcal{L}_0 = 10m$, $h = 1000m$. The diaphragm width was taken equal to few arc-seconds.

The spatial coherence parameters r_0 and $\mathcal{L}_0$ may be obtained with the pupil-plane observation way together with AA fluctuation characteristic times. The structure function of AA fluctuations recorded by mean of a pair of photodiodes positioned in the pupil image may be expressed as:[16]

$$d_\alpha(s) = 0.364[1 - k(\frac{s}{D_p})^{-\frac{5}{3}}]\lambda^2 r_0^{-\frac{5}{3}} D_p^{-\frac{5}{3}} \tag{11}$$

where k is a constant respectively equal to 0.541 or 0.810 according that we consider AA projected on the baseline formed by the photodiodes separated by the distance s or onto a perpendicular direction. D_p is the area integration size of the photodiodes. Equation 11 will be used to calculate r_0.

The spatial coherence outer scale $\mathcal{L}_0$ may be deduced from Equation 2 for θ equal 0. The integration gives in this case and considering that $\mathcal{L}_0$ is great in regard to D_p:[17]

$$\mathcal{C}_\alpha(0, D_p) = 0.017\lambda^2 r_0^{-\frac{5}{3}}\left[D_p^{-\frac{1}{3}} - 1.525\mathcal{L}_0^{-\frac{1}{3}}\right] \tag{12}$$

The $\mathcal{L}_0$ parameter will be obtained from Equation 12 applied to 2 photodiodes of different area integration sizes D_{p_1} and D_{p_2}. It will be obtained from the ratio $r_{\mathcal{L}_0}$:

$$r_{\mathcal{L}_0} = \frac{\mathcal{C}_\alpha(0, D_{p_1}) - \mathcal{C}_\alpha(0, D_{p_2})}{\mathcal{C}_\alpha(0, D_{p_1})} = \frac{D_{p_1}^{-\frac{1}{3}} - D_{p_2}^{-\frac{1}{3}}}{D_{p_1}^{-\frac{1}{3}} - 1.525\mathcal{L}_0^{-\frac{1}{3}}} \tag{13}$$

5. SOME FIRST RESULTS

Some preliminary results are presented in this section. They are obtained from an analysis performed on solar data recorded with the image-plane observation way. Data consist in image series of about 2400 samples recorded at a rate of 30 per seconds. The figure 4 shows an image of the Sun recorded March 15, 2010 with this observation way. Its size is approximately 96 by 128 arc-seconds. Each CCD pixel line in the direct and reflected limb images
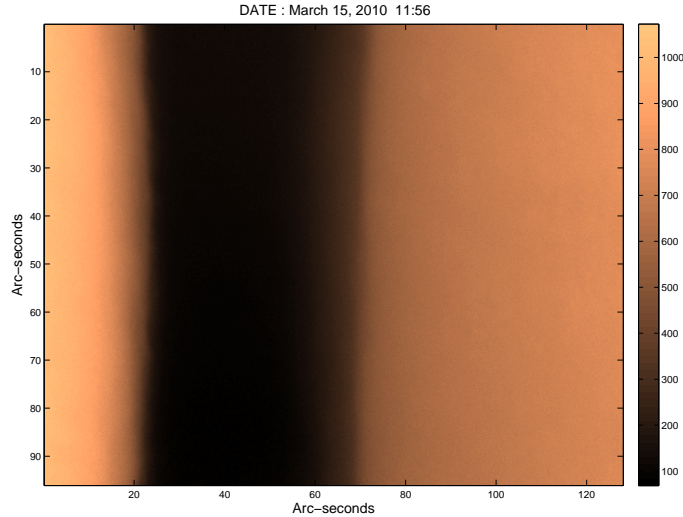

Figure 4. A solar image obtained with the image-plane observation way of MISOLFA.

are such as they are located on a direction parallel to the horizon. AA-fluctuations are extracted from temporal series of solar images allowing to compute the experimental covariance function $\mathcal{C}_{\alpha Exp}(\theta)$ and the structure function $d_{\alpha Exp}(\theta)$ from Equation 4. The Fried parameter r_0, the spatial coherence outer scale $\mathcal{L}_0$ and the altitude of the equivalent impulse layer h are then estimated fitting $d_{\alpha Exp}(\theta)$ with the theoretical model given by Equation 3. Figure 5 shows the parameter estimation obtained from sequences recorded December 9, 2010 at 09:26 and December 14, 2010 at 12:36. The Fried parameter r_0, the spatial coherence outer scale $\mathcal{L}_0$ and the impulse layer altitude h have been found respectively equal to 2.7 cm, 4091 m and 8791 m and 5.3 cm, 7014 m and 7405 m. We can see that the value of $\mathcal{L}_0$ are large allowing to considerer the Kolmogorov model for r_0 estimation:[1, 18]

$$r_0 = 8.25 \ 10^5 \lambda^{\frac{6}{5}} D^{-\frac{1}{5}} \sigma_\alpha^{-\frac{6}{5}} \tag{14}$$

where the standard deviation σ_α is expressed in arc-seconds in Equation 14.

Equation 14 have been used to compute Fried's parameter from the same data sets. The results are shown on
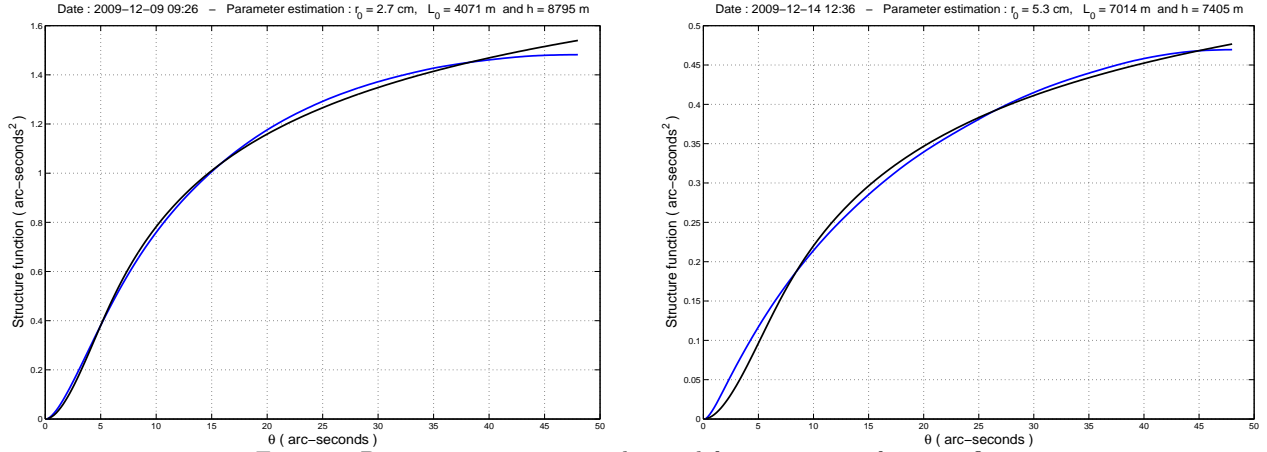
Figure 5. Parameter estimations obtained from structure function fits

figure 6. Two cases were considered. In the first one, the standard deviation σ_α of AA-fluctuations is computed considering the fluctuations of the solar limb position on the central line of the direct image integrated over increasing time intervals up to 80 seconds. This case is shown on the top of figure 6. In the second case, the standard deviation of the limb position is always calculated over duration of 2 seconds i.e. we divide the whole temporal signal of limb positions in short samples of equal duration. The result is shown on the bottom
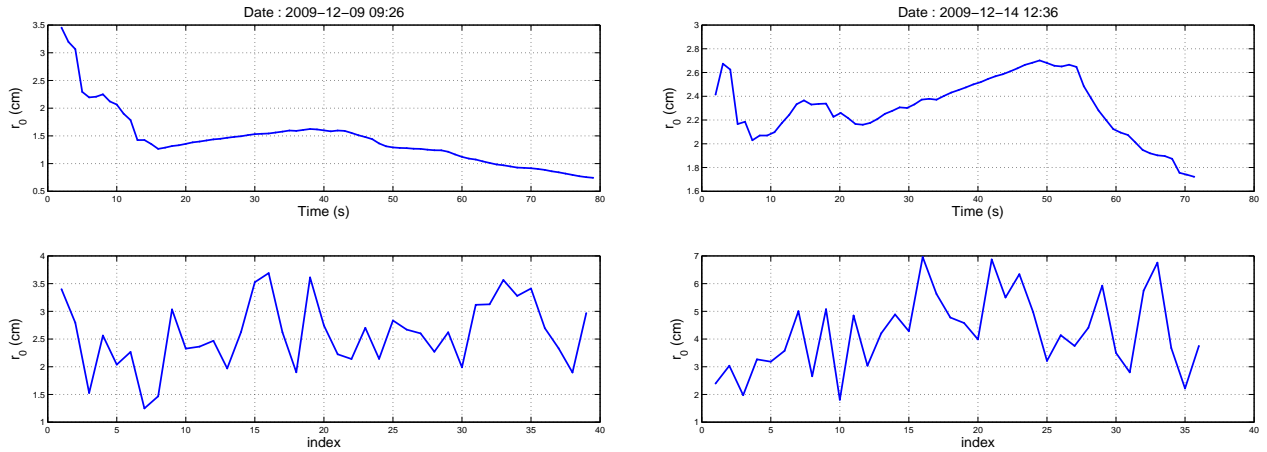

Figure 6. Fried's parameter estimation

in the figure 6. We observe that the temporal length of the sample is an important factor when we want to estimate the turbulence parameter. It seems that the parameters are better estimated when short samples are considered. This is probably due to the presence of different regimes in the atmosphere which overlap during daytime observations. The stationarity assumption may not be always respected. The r_0 mean value obtained with short temporal samples is equal the one obtained when fitting the experimental structure function with the theoretical model (see figure 5). Finally, we calculated the Fried parameter versus θ at different sampling time considering the direct and reflected limb images. Comparing the two opposite limb images correspond to large angular distance of approximately 1880". The time reference is the beginning of data recording. The others considered limbs are separated from the reference by a time step $\Delta\theta_T$ of 20, 40 and 60 seconds. The figure 7 shows the obtained results from the two considered observation days. We see that we may have in poor seeing conditions r_0 variations of several centimeters in short periods of time and at all angular scales (left part figure 7). Theses variations may be more structured at large angular scales when the seeing is better (right part figure 7).
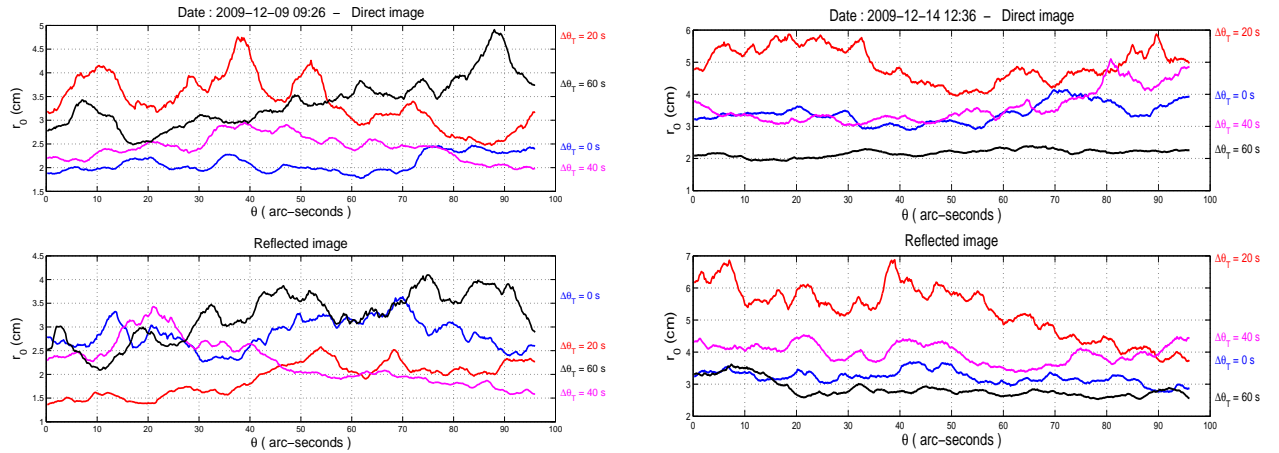
Figure 7. Fried's parameter versus at different sampling time θ

6. CONCLUSION

The Generalized Solar Seeing Monitor MISOLFA is developed in the context of the next launch of the spatial mission PICARD. It will observe near the replica of the space instrument installed at Calern Observatory (Observatoire de la Côte d'Azur - France). It will be useful to link the solar diameter measurements performed from space and from ground level and to better understand atmospheric optical properties. The MISOLFA experimental concept based on AA statistics, will allow to estimate all parameters associated to the perturbed wavefronts (Fried's parameter r0, spatial coherence outer scale $\mathcal{L}_0$, isoplanatic angle θ_0, the characteristic coherence time τ_0 and the vertical optical turbulence profile $C_n^2(h)$ in the framework of a turbulence model. Indeed, the observation of the AA fluctuations, simultaneously in the image and the pupil planes, leads to a complete information on the coherence status of the wavefronts as well as on the localization of the atmospheric turbulence via the variances, covariances (or structure functions). It could also allow to propose eventually a more realistic modelling.

ACKNOWLEDGMENTS

REFERENCES

[1] A. Irbah, F. Laclare, J. Borgnino and G. Merlin,*Solar Phys.*, 149, 213, 1994.
[2] L. Lakhal, A. Irbah, M. Bouzaria, J. Borgnino, F. Laclare, C. Delmas, *Astron. Astrophys. Suppl. Ser.*, 138, 155, 1999.
[3] G. Thuillier, S. Dewitte, W. Schmutz and the PICARD team, *Advance Space Research*, 38, 1792, 2006.
[4] T. Corbard, P. Boumier,T. Appourchaux, S.J. Jiménez-Reyes, B. Gelly and the PICARD team, *Astron. Nachr.*, 329, No. 5, 508 - 516, 2008.
[5] P. Assus, A. Irbah, P. Bourget, T. Corbard and the PICARD team, *Astron. Nachr.*, 329, No. 5, 517 - 520, 2008.
[6] A. Irbah, J. Borgnino, F. Laclare, and G. Merlin, "Isoplanatism and high spatial resolution solar imaging," *Astron. Astrophys.*, 276, pp. 663–672, 1993.
[7] F. Martin, A. Tokovinin, A. Agabi, J. Borgnino and A. Ziad, *Astron. Astrophys. Suppl. Ser.*, 108, pp. 173–180, 1994.
[8] A. Ziad, R. Conan, A. Tokovinin, F. Martin, and J. Borgnino "From the Grating Scale Monitor to the Generalized Seeing Monitor," *Applied Optics* **39**, p. 30, 2000.

[9] R. Avila, A. Ziad, J. Borgnino, F. Martin, A. Agabi and A. A. Tokovinin, "Theoretical spatio-temporal analysis of angle of arrival induced by atmospheric turbulence as observed with the Grating Scale Monitor Experiment," *J. Opt. Soc. Amer. A* **14**, p. 11, 1997.

[10] N. Seghouani, A. Irbah and J. Borgnino, Marrakech Site 2000, Astronomical Site Evaluation in the Visible and Radio Range, Marrakech - Morocco, November 13-17, 2000.

[11] A. Bouzid, A. Irbah, J. Borgnino J. and H. Lantri H., Marrakech Site 2000, Astronomical Site Evaluation in the Visible and Radio Range, Marrakech - Morocco, November 13-17, 2000.

[12] J. Borgnino, and F. Martin, "Analyse statistique des déformations aléatoires d'une surface d'onde dues à la turbulence atmosphérique au voisinage du sol, I.- Exposé de la méthode, Premiers résultats," *J. Optics (Paris)* **8**, pp. 319–326, 1977.

[13] J. Borgnino, and F. Martin, "Analyse statistique des déformations aléatoires d'une surface d'onde dues à la turbulence atmosphérique au voisinage du sol, II.- Estimation des fonctions de corrélation par traitement numérique," *J. Optics (Paris)* **9**, pp. 15–24, 1977.

[14] A. Berdja, A. Irbah , J. Borgnino and F. Martin , "Simulmation of pupil-plane observation of angle-of-arrival fluctuations in daytime turbulence, in Optics in Atmospheric", Propagation and Adaptive Systems VI, edited by John D. Gonglewski and Karin Stein, Proceedings of SPIE Vol. 5237 (SPIE, Bellingham, WA, 2004), p. 238-248, 2004

[15] J. Borgnino, A. Berdja, A. Ziad and J. Maire, "An Optical Turbulence Profiler for the terrestrial atmosphere boundary-layer", Proceedings of Symposium of Seeing, Kona, Hawaii, 20-22 March 2007, T. Cherubini and S. Businger, eds., 2007

[16] M. Sarazin and F. Roddier, The ESO differential image motion monitor, Astron. and Astrophys., 227, p. 294-300, 1990

[17] A. Ziad , J. Borgnino , F. Martin and A. Agabi , "Experimental estimation of the spatial coherence outer scale from a wavefront statistical analysis", Astron. and Astrophys. 282, p. 1021-1033, 1994

[18] J. Borgnino, G. Ceppatelli, G. Ricort and A. Righini, Astron. Astrophys. 107, 333, 1982